DSMC Analysis of Pressure Effect on Low-Density Nozzle Flow

Chan-Hong Chung* and Kyung-Hoe Kim*
Department of Chemical Engineering
Taegu University, Kyungbuk Kyungsan, Korea 712-714

Abstract

The flow in low-density plumes expanding into a region of finite pressure shows a quite different behavior from that observed in low-density plumes expanding into a vacuum. The flow structure in the plume varies depending on applied ambient and stagnation chamber conditions. In the present study, the direct simulation Monte-Carlo (DSMC) method based on molecular gas dynamics is employed in the analysis of low-density gas flows expanding through a small converging/diverging nozzle. Special attention has been paid to the effect of non-zero ambient and stagnation pressures on the flow structure which has rarely been studied using the DSMC method.

Key Word : nozzle flow, rarefied gas flow, plume, DSMC method

Introduction

Low-thrust rocket engines which are used for station keeping and altitude control have a significant impact on the mission performance such as on-orbit lifetimes, payloads, and trip times of satellites and spacecraft. Another important factor affecting the mission performance is the contamination of sensitive instruments and system components of the vehicles in the plume and backflow region of the thrusters. Hence, understanding of the detailed flow structure around low-thrust rocket nozzles is very important not only for the accurate prediction of the thrust and mass flow levels but also for the precise analysis of the plume and backflow region.

The low-density flow through small nozzles expanding into a vacuum has been examined previously both in experimental and in numerical investigations. Few experimental data are available for this type of low-thrust nozzle and most data deal with gross characteristics of nozzle performance such as thrust levels and discharge coefficients. This data does not provide detailed information regarding the flow structure inside the nozzle and in the plume. Rothe[1,2] measured detailed low-density flow properties such as density and temperature distributions in a low-thrust nozzle using the electron-beam fluorescence technique. Rothe's experiment was numerically investigated by Chung *et al.* [3,4] using a continuum CFD code based on the Navier-Stokes equations and the direct-simulation Monte-Carlo (DSMC) method of Bird[5]. They[3] compared simulation results with Rothe's density and rotational temperature data at various locations inside the nozzle and at the nozzle exit plane. They[4] also showed that the DSMC method can successfully predict the presence of a Mach disk and a barrel-shaped shock, which are representative of overexpanded nozzle plumes. In addition to Rothe's work, low-density pitot pressure measurements together with numerical simulations were performed by Penko and Boyd[6,7]. Campbell *et al.*[8] and Zelesnik *et al.*[9] have also analyzed expanding low-density flows using the DSMC method and compared their results with experimental data.

---

* Professor

For this type of rocket engine, due to the small thrust level, nozzle scales are quite small and reservoir pressures are very low. Reynolds numbers of the flow in the nozzle are very low and rarefaction effects can significantly alter the internal flow structure in the space environment. Under these conditions, the flow exhibits strong nonequilibrium effects, such as slip at the wall, due to rapid expansion into the low-density environment. The fluid experiences continuum, transition, and free-molecular flow regimes. Consequently, conventional continuum gas dynamics may not be adequate and an approach based on molecular gas dynamics is required for the analysis of the flow.

Of the various methods available for the analysis of low-density gas flows, the DSMC method is the one that is most widely used and readily applicable. The DSMC method is a computer simulation technique to solve the Boltzmann equation by modeling a real gas flow using a representative set of molecules. Theoretically, the DSMC method can be applied to any flow for which the Boltzmann equation is valid. However, due to intensive computational requirements, current applications of the DSMC method are generally limited to near continuum and rarefied flows. Continuum methods are usually much more efficient than the DSMC method for high and normal density flows. Thus, in the analysis of flows which involve both continuum and rarefied flow regimes, it would be reasonable to combine both methods. The simplest utilization of both methods is to solve rarefied flow regimes using the DSMC method by obtaining boundary conditions from the solution of continuum methods. This, indeed, is the most widely used method in analyzing flows which involve both continuum and rarefied flow regimes.

In the present study, the DSMC method based on molecular gas dynamics is employed in the analysis of low-density gas flows expanding through a small converging/diverging nozzle. Special attention has been paid to the effect of non-zero ambient and stagnation chamber pressures on the flow structure, which has rarely been studied using the DSMC method. In contrast to the behavior observed in low-density plumes expanding into a vacuum, the flow in low-density plumes expanding into a region of finite pressure shows a complicated flow pattern depending on applied ambient and stagnation chamber pressures.

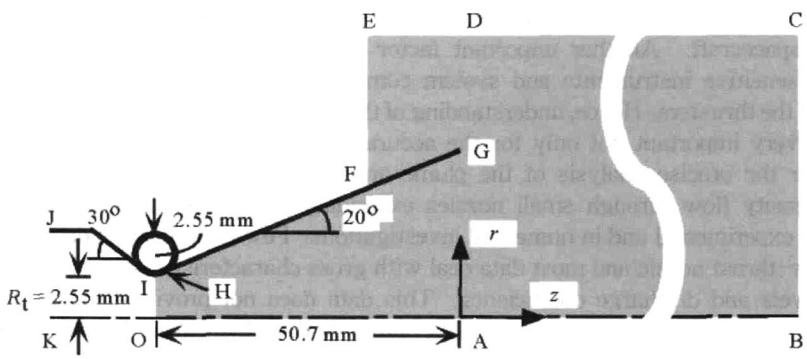

Fig. 1. Low-thrust nozzle and simulation domain.

Problem Statement

For the analysis of low-density nozzle flow, Rothe's[1,2] experiment is chosen as a reference problem. Figure 1 illustrates the geometry of the nozzle used in Rothe's experiment and in the present numerical analysis. The nozzle is made of graphite to reduce optical reflections and to minimize back-scattering and secondary emission of electrons. The subsonic and supersonic portions of the nozzle are cones having half-angles of 30^o and 20^o, respectively, with longitudinal radii of curvature at the throat equal to 1/2 of the throat radius. The maximum area ratio at the exit based on the

throat area is 66. The shaded region in Fig. 1 indicates the DSMC simulation domain. The length of the curved nozzle contour (IH) is about 0.5 mm. The inflow boundary is located at the nozzle throat (OI). The inflow boundary condition is obtained from the solution of the Navier-Stokes equations[3]. The simulation domain extends an axial distance of 260 mm from the nozzle exit plane (BC), a radial distance of 50 mm from the nozzle lip (EC), and an axial distance of 20 mm from the nozzle exit plane into the backflow region (EF). The radial and downstream boundaries are located far enough from the nozzle exit so that a further change in the location of the boundaries does not result in any significant changes in the macroscopic flow variables in the plume. Along the boundaries CE and EF an equilibrium condition corresponding to the ambient condition is used as the boundary condition. Along the boundary BC an equilibrium condition corresponding to a profile extrapolated from the inside of the plume is used as the boundary condition. Details regarding the boundary conditions may be found in Ref. 4. The test gas is nitrogen with a stagnation temperature of T_o = 300 K. Rothe's experimental flow conditions, which are employed in the present numerical analysis as well, are listed in Table 1. In the table, the throat Reynolds number, $R_{e,t} = 2\dot{m}/\pi\mu_o R_t$, is based on the viscosity at the stagnation chamber condition, μ_o. Here the quantity $\dot{m}$ is the mass flow rate based on the adiabatic escape speed[1] $u = \sqrt{2H_o}$ and R_t is the throat radius. The Knudsen number Kn is based on the throat diameter and the stagnation chamber condition.

Table 1. Flow conditions

	Case I	Case II	Case III	Case IV
Test gas	N_2	N_2	N_2	N_2
Stagnation Temperature, T_o	300 K	300 K	300 K	300 K
Stagnation Pressure, P_o	140 Pa	88 Pa	474 Pa	1245 Pa
Wall temperature, T_W	300 K	300 K	300 K	300 K
Reynolds number, $R_{e,t}$	80	50	270	709
Knudsen number, Kn	7.8×10^{-3}	1.2×10^{-2}	2.3×10^{-3}	8.8×10^{-4}
Ambient pressure, P_b	*	0.37 Pa	1.8 Pa	3.8 Pa

DSMC Method

The DSMC method is a popular simulation technique for low-density flows and the DSMC code used in the present study is based on the same principles as described in Bird [5], together with the variable hard sphere (VHS) model[10] as a molecular model and the no time counter (NTC) method[11] as a collision sampling technique. The code has been applied to various low-density flows of gas mixtures in arbitrary shaped flow domains[3,4,12,13]. Details of the code may be found in Ref. 3.

The VHS exponent, ω, of nitrogen is chosen to be 0.24 with the reference molecular diameter of 4.07×10^{-10} m at the reference temperature 273K[10]. Chemical reactions and the vibrational mode are assumed to be frozen. For the calculation of rotational energy exchange between the colliding molecules, the Borgnakke-Larsen phenomenological model[14] is employed together with the temperature-dependent energy exchange probability of Boyd[15] modified by Chung *et al.*[3] to be consistent with the experimental data for the rotational relaxation of nitrogen obtained by various methods and compatible with the VHS model. A diffusely adiabatic wall with 10% thermal accommodation is assumed for the interaction between the gas molecules and the wall. Details regarding the wall boundary condition may be found in Ref. 3.

Results and Discussion

To present the general idea regarding the underexpanded low-density nozzle plumes and the effect of ambient pressures on the structure of the flowfield, a relatively low Reynolds number flow will be considered first. Figures 2-5 show the effect of ambient pressures on the flowfield for Case I in which the stagnation pressure is 140 Pa.

In Fig. 2, density variations along the centerline are compared with Rothe's experimental data. In the results from the DSMC method, the density variation along the centerline for three different background pressures (0.54 Pa, 0.15 Pa, and vacuum) is shown for comparison. The density is normalized by the stagnation chamber density. Rothe's experimental data was obtained for a background pressure of 0.52 Pa (P_b/P_o = 0.004). In this case of underexpanded nozzle flow, the density decreases from the throat to the nozzle exit and approaches the background density in the plume. The simulation results indicate that for the three different ambient conditions, the density profiles along the axis show no significant differences inside the nozzle for the case where the stagnation pressure P_o = 140 Pa.

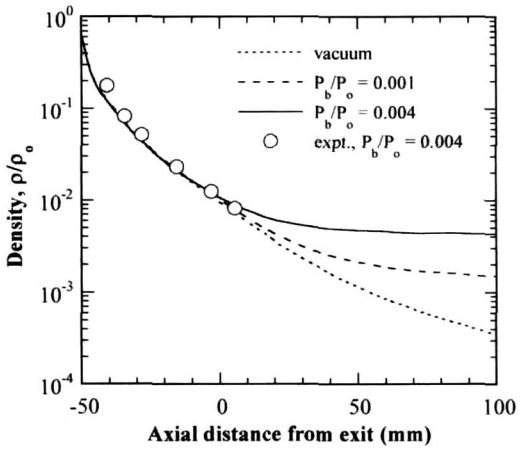

Fig. 2. Density distribution along the axis.

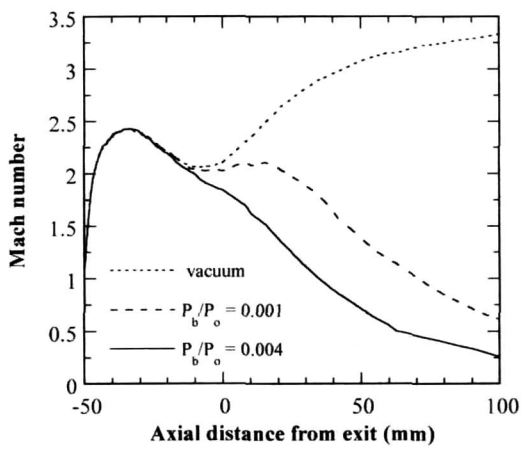

Fig. 3. Mach number distribution along the axis.

The Mach number distribution along the axis of the nozzle is depicted in Fig. 3. Inside the nozzle, the three Mach numbers are nearly the same and are not influenced by the external condition. The Mach numbers increase from the throat and show local maximum inside the nozzle. The maximum Mach number is about 2.45 and occurs just 15 mm downstream from the throat. After the local maximum, the Mach numbers decrease. Around the nozzle exit the flow starts to adjust to the ambient condition. In case of the flow expanding into a vacuum, the Mach number shows a local minimum around the nozzle exit and then increases. At the higher background pressure of P_b = 0.54 Pa (P_b/P_o = 0.004), the Mach number continues to decrease. At the lower background pressure of P_b = 0.15 Pa (P_b/P_o = 0.001), the Mach number shows a local minimum similar to that of the flow expanding into a vacuum. In this case, however, the expansion is suppressed by the ambient gas and the Mach number decreases. It should be noted that the local maximum Mach numbers in the present cases are not a shock wave which can be observed in overexpanded plumes. In a shock wave observed in overexpanded plumes, Mach number decreases while flow decelerates and density increases. In the present cases, however, the flow continues to accelerate and the density decreases as shown in Fig. 2. The existence of local maximum Mach number inside the nozzle in the present cases is the result of the increase of temperature due to an increase of the flow energy by viscous dissipation which will be shown in the next figure.

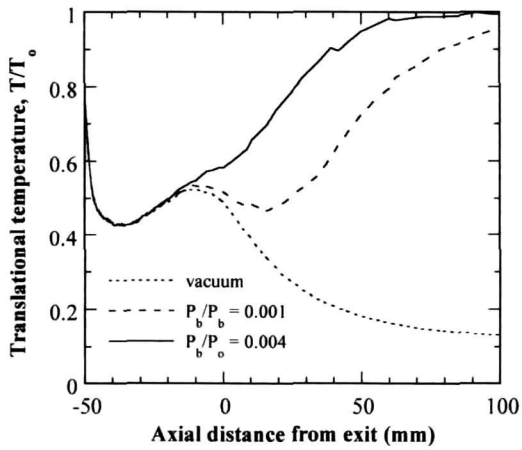

Fig. 4. Translational temperature distribution along the axis.

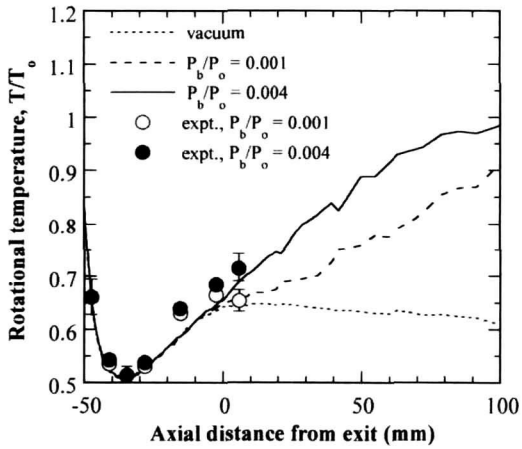

Fig. 5. Rotational temperature distribution along the axis.

Figure 4 shows translational temperature distribution along the axis of the nozzle for the three different background pressures. The temperatures are normalized by the stagnation temperature. It can be seen that the translational temperatures pass through a local minimum and then increase toward the nozzle exit due to rarefaction effects. This is because the effect of molecule-surface collisions becomes as important as that of molecule-molecule collisions in these low-density flows. That is, as the flow becomes more rarefied, the molecules which have collided on the hotter nozzle surface can easily reach the axis of the nozzle where the temperature is lower without losing their energy by collisions with other molecules. In case of the flow expanding into a vacuum, the translational temperature shows local maximum around the nozzle exit and decreases in the plume due to geometrical expansion. Far downstream, the translational temperature becomes almost frozen due to the rapid expansion into a vacuum. For the case of the higher background pressure of P_b = 0.54 Pa(P_b/P_o = 0.004), the flow quickly adjusts to the ambient gas and the translational temperature increases until it reaches the ambient temperature. For the case of the lower background pressure of P_b = 0.15 Pa(P_b/P_o = 0.001), the translational temperature decreases as is the case in the flow expanding into a vacuum. Then, the translational temperature passes through one more local minimum before it increases due to the adjustment to the ambient gas.

In Fig. 5, rotational temperature distribution along the axis of the nozzle is compared with Rothe's experimental data. The variations of the rotational temperatures are quite similar to those of the translational temperatures except that the rate of change is more gradual than that of the translational temperatures. This is because the exchange of rotational energy is less efficient than that of the translational energy. The rotational temperatures also pass through a local minimum and then increase toward the nozzle exit. In case of the rotational temperatures, the local minimum value is about 52% of the stagnation temperature while that of the translational temperatures is about 43%. In case of the flow expanding into a vacuum, the minimum value around the exit is about 65% of the stagnation temperature. In the plume, the rotational temperature becomes frozen faster than the translational temperature. For the case of the lower background pressure of P_b = 0.15 Pa, the rotational temperature does not pass through a secondary local minimum.

Consideration is now given to the effect of stagnation pressures. To investigate the effect of stagnation pressures on the structure of the flowfield, three different cases with the same stagnation temperature T_o = 300 K are considered: (1) stagnation pressure P_o = 88 Pa and ambient pressure

P_b = 0.37 Pa (Case II); P_o = 474 Pa and P_b = 1.8 Pa (Case III); and P_o = 1245 Pa and P_b = 3.8 Pa (Case IV). For the three cases, the ratio of the stagnation to the ambient pressures is in a range from 240 to 325.

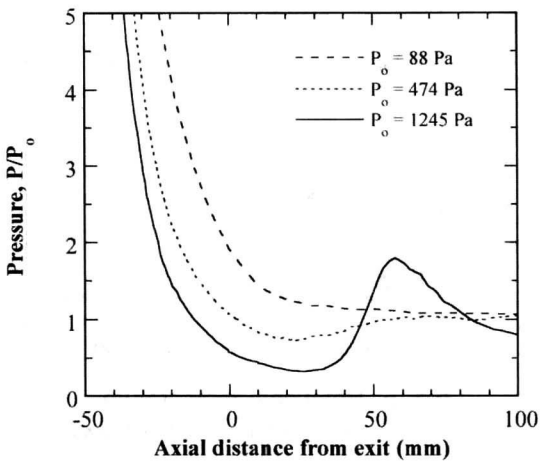

Fig. 6. Effect of stagnation pressure on the centerline pressure.

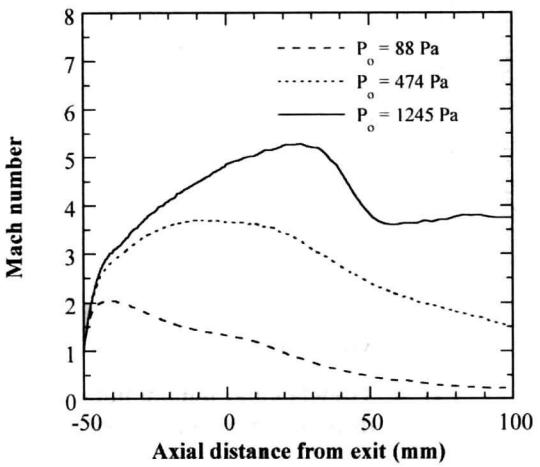

Fig. 7. Effect of stagnation pressure on the Mach number distribution along the axis.

The pressure distribution along the axis of the nozzle is depicted in Fig. 6, which shows the extent of expansion in the plume. In the figure, the pressure is normalized by the ambient pressure. In case of the lowest stagnation pressure of P_o = 88 Pa, the pressure decreases from the throat to the nozzle exit and approaches the background pressure in the plume. For the stagnation pressure of P_o = 474 Pa, the flow is slightly overexpanded just outside the nozzle exit. However, the overexpansion is not strong enough to cause any significant disturbances and the flow quickly adjusts to the ambient pressure. For the highest stagnation pressure of P_o = 1245 Pa, it can be seen that the flow is overexpanded. The centerline pressure at the exit is about 60% of the ambient pressure and drops to 33% of the ambient pressure at 25 mm downstream from the exit. In the plume, back pressure effects cause the flow to turn into the axis and produce the characteristic barrel-shock configuration. Beyond the shock, the flow expands again. Although not shown, the expansion in this time is not strong enough to sustain the repetitive pattern of expansion.

The Mach number distribution along the axis of the nozzle is depicted in Fig. 7. In case of the lowest stagnation pressure of P_o = 88 Pa, the Mach number shows a local maximum inside the nozzle. The maximum Mach number is about 2.0 and occurs just 10 mm downstream from the throat. For the stagnation pressure of P_o = 474 Pa, the Mach number increases from the throat to the nozzle exit. Maximum Mach number is about 3.7 and occurs just inside the nozzle near the exit. In these two cases, the Mach numbers continue to decrease after the local maximum. For the highest stagnation pressure of P_o = 1245 Pa, there is no local maximum inside the nozzle. The maximum Mach number is about 5.2 and occurs about 25 mm downstream from the exit where the pressure becomes minimum. After the maximum, the Mach number drops to about 3.7 and shows a very weak repetitive pattern of expansion. This is a shock wave which is different from the local maximum due to viscous dissipation in the lower stagnation pressure cases. By comparing the results with those in Fig. 3, it can be seen that as the stagnation pressure decreases, the maximum Mach number decreases and the location moves toward the throat in the underexpanded flows.

The density distribution along the axis of the nozzle for the three different cases is shown in Fig. 8. For the lower stagnation pressures of P_o = 88 Pa and 474 Pa, the densities decrease from the throat to the nozzle exit and approach the background densities far downstream. In case of the highest stagnation pressure of P_o = 1245 Pa, the density decreases inside the nozzle but shows a minimum in the plume. The local minimum density is about 2.2 times the ambient density and occurs about 25 mm downstream from the exit in the plume where the pressure is minimum and the Mach number is maximum. After the local minimum, the density increases across the shock wave until a local maximum occurs. The local maximum density is about 6.4 times the ambient density and occurs about 35 mm downstream from the local minimum.

Finally, comparison of rotational and translational temperatures for the three cases is shown in Fig. 9, which shows the degree of thermal nonequilibrium inside the nozzle and in the plume. It can be seen that, from the rapid expansion, the rotational temperatures are always higher than the translational temperatures along the axis inside the nozzle and in the near plume. It also can be seen that as the stagnation pressure decreases, *i.e.*, as the flow becomes more rarefied, the degree of thermal nonequilibrium increases. In case of the lowest stagnation pressure of P_o = 88 Pa, the translational and rotational temperatures show local minimums about 10 mm downstream from the throat inside the nozzle and then increase to the exit due to viscous dissipation. In the plume, the translational temperature becomes higher than the rotational temperature. For the stagnation pressure of P_o = 474 Pa, the viscous dissipation is not strong enough to increase the temperatures along the axis inside the nozzle. The minimum temperature occurs just inside the nozzle near the exit. For the highest stagnation pressure of P_o = 1245 Pa, the translational temperature becomes higher than the rotational temperature across the shock wave from rapid compression. Beyond the shock, the rotational temperature is higher than the translational temperature where the flow once again expands.

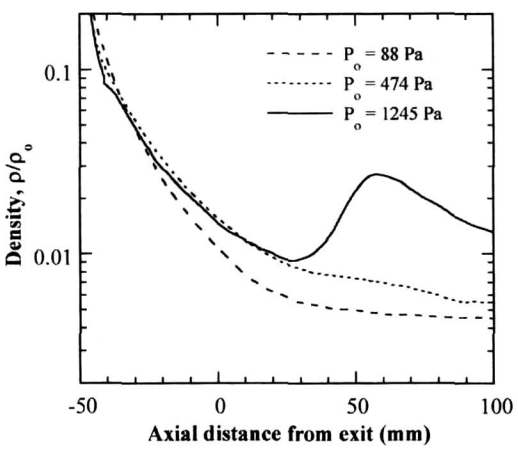

Fig. 8. Effect of stagnation pressure on the density distribution along the axis.

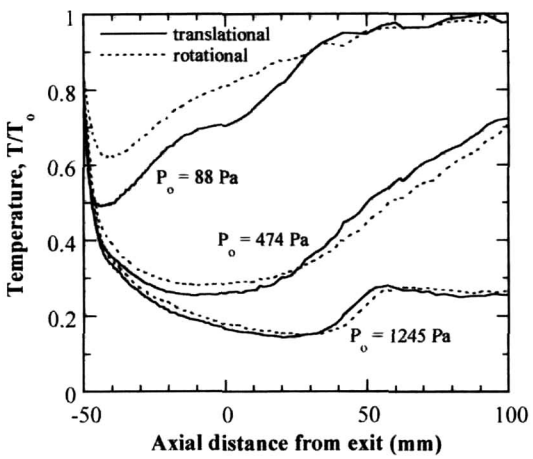

Fig. 9. Effect of stagnation pressure on the temperature distribution along the axis.

Conclusions

The flow structure in low-density plumes expanding through a small converging/diverging nozzle into a region of finite pressure is investigated using the direct simulation Monte-Carlo (DSMC) method based on molecular gas dynamics. This kind of flow structure has rarely been studied using

the DSMC method. The simulation results show good agreement with Rothe's experimental data inside the nozzle. The calculated results show that in contrast to the behavior observed in low-density plumes expanding into a vacuum the flow in low-density plumes expanding into a region of finite pressure shows a complicated flow pattern depending on applied ambient and stagnation chamber pressures.

Acknowledgement

This research was supported(in part) by the Taegu University Research Grant, 2000.

References

1. Rothe, D. E., "Electron Beam Studies of Viscous Flow in Supersonic Nozzles," AIAA J., Vol. 9, No. 5, 1972, pp. 804-811.

2. Rothe, D. E., Experimental Study of Viscous Low-Density Nozzle Flows, AI-2590-A-2, Cornell Aeronautical Lab., Inc., Buffalo, New York, June 1970.

3. Chung, C. H., Kim, S. C., Stubbs, R. M., and De Witt, K. J., "Analysis of Low-Density Nozzle Flow by the Direct Simulation Monte-Carlo and Continuum Methods," J. Propulsion and Power, Vol. 11, No. 1, 1995, pp. 64-70.

4. Chung, C. H., De Witt, K. J., Stubbs, R. M., and Penko, P. F., "Simulation of Overexpanded Low-Density Nozzle Plume Flow," AIAA J., Vol. 33, No. 9, 1995, pp. 1646-1650.

5. Bird, G. A., Molecular Gas Dynamics, Oxford University Press, London, 1976.

6. Penko, P. F., Boyd, I. D., Meissner, D. L., and DeWitt, K. J., "Pressure Measurements in a Low-Density Nozzle Plume for Code Verification," AIAA Paper 91-2110, June, 1991.

7. Boyd, I. D., Penko, P. F., Meissner, D. L., and De Witt, K. J., "Experimental and Numerical Investigations of Low-Density Nozzle and Plume Flows of Nitrogen," AIAA J., Vol. 30, No. 10, 1992, pp. 2453-2461.

8. Campbell, D. H., Wysong, I. J., Weaver, D. P., and Muntz, E. P., "Flowfield Characteristics in Freejets of Monatomic and Diatomic Gases," Progress in Astronautics and Aeronautics: Rarefied Gas Dynamics, edited by B. D. Shizgal and D. P. Weaver, Vol. 158, AIAA, Washington, DC, 1994, pp. 90-97.

9. Zelesnik, D., Dunn, T., Micci, M. M., and Long, L. N., " Numerical and Experimental Investigation of Low Reynolds Number Nozzle Flows," AIAA Paper 91-3558, September, 1991.

10. Bird, G. A., "Monte Carlo Simulation in an Engineering Context," Progress in Astronautics and Aeronautics: Rarefied Gas Dynamics, edited by Sam S. Fisher, Vol. 74, Part I, AIAA, New York, 1981, pp. 239-255.

11. Bird, G. A., "The Perception of Numerical Methods in Rarefied Gas Dynamics," Progress in Astronautics and Aeronautics: Rarefied Gas Dynamics, edited by E. P. Muntz, D. P. Weaver, and D. H. Campbell, AIAA, Washington, DC, Vol. 118, 1989, pp. 211-226.

12. Chung, C. H., Kim, S. C., Stubbs, R. M., and De Witt, K. J., "Analysis of Plum Backflow Around a Nozzle Lip in a Nuclear Rocket," AIAA Paper 93-2497, June 1993.

13. Chung, C. H., Kim, S. C., De Witt, K. J., and Nagamatsu, H. T., "Numerical Analysis of Hypersonic Low-Density Scramjet Inlet Flow," J. Spacecraft and Rockets, Vol. 32, No. 1, 1995, pp. 60-66.

14. Borgnakke, C. and Larsen, P. S., "Statistical Collision Models for Monte Carlo Simulation of Polyatomic Gas Mixture," J. Computational Physics, Vol. 18, 1975, pp. 405-420.

15. Boyd, I. D., "Analysis of Rotational Nonequilibrium in Standing Shock Waves of Nitrogen," AIAA J., Vol. 28, No. 11, 1990, pp. 1997-1999.